https://doi.org/10.48048/tis.2022.4623

Dynamic Displacement using DInSAR of Sentinel-1 in Sunda Strait

Argo Galih Suhadha[1,2,*] and Atriyon Julzarika[2,3]

[1]National Research and Innovation Agency (BRIN), Jakarta, Indonesia
[2]Department of Geodetic Engineering, Universitas Gadjah Mada, Yogyakarta, Indonesia
[3]Research Center for Geospatial, National Research and Innovation Agency (BRIN), Cibinong, Indonesia

([*]Corresponding author's e-mail: agsuhadha@gmail.com)

Received: 1 March 2021, Revised: 22 June 2021, Accepted: 22 July 2021

Abstract

Sunda Strait's geographical condition makes it experience many tectonic and seismic events. Deformation monitoring has been carried out with various methods ranging from terrestrial and non-terrestrial surveys. This study aimed to monitor the dynamics of deformation in the Sunda Strait region in 2019 using Differential Interferometric Synthetic Aperture Radar (DInSAR). DInSAR principle analyzes the paired SAR images that have been co-registered with different acquisition times to detect changes along the sensor observation line to the target or Line of Sight (LOS). The SAR data used are Sentinel-1 acquisition on June 1, and October 23, 2019. The results show that the coherence value of the image pair is low due to differences in the phase and intensity values. The maximum uplift value is 0.54 m located in the West Lampung Regency, and the subsidence is −0.3 m in the Pesisir Barat Regency. Uplift results are located in various geological conditions and do not affect by seismic phenomena, whereas subsidence shows its location in the potential area of land subsidence. The dynamics of uplift and subsidence in the Lampung regency are mostly affected by the geological and land use conditions of the locations.

Keywords: DInSAR, Displacement, LOS, Subsidence, Sunda strait, Uplift

Introduction

Sunda Strait, which is a strait located on the subduction zone among Java Island and Sumatera Island, has a complex tectonic structure and experienced seismic activity for the last 40 years (**Figure 1**). This region is in the changing of the subduction system from the oblique subduction transitional zone between the Eurasian Plate and the Indo-Australian plate along the Sumatra Island to the frontal subduction of Java [1]. Furthermore, Sunda Strait has one of the most active faults in the world and has caused the formation of large lakes on Sumatra Island, including a combination of tectonic and volcanic activity [2]. The historical intensity of earthquake events in the Sunda Strait indicates that this region has a potential recurrence of the earthquake and tsunami effects from the subduction zone [3,4].

The subduction zone is well defined by the existence of Mount Anak Krakatau which is part of the stretched volcanic arc about 6,000 km from Sumatra, the southern part of West Java to the Molucca Sea [5]. There is also the Semangko Fault in the Sunda Strait, which is part of the Sumatran Fault Zone along the 1,650 km and contributes to 40 % of the parallel displacement compound of the Sumatra Fault Zone [6]. This condition implies that Sunda Strait has a high potential for tsunamis events. The latest tsunami occurred on December 22, 2018, which was thought to be a result of the eruption of Mount Anak Krakatau. The eruption which resulted from the nature flank failure controlled by the internal structure of the island generates that tsunami [7].

The number of tectonic and seismic events in the Sunda Strait resulted in high geodynamics in the region. Ground deformation in terms of land subsidence, uplift, or landslides is un-periodic and irreversible, caused by seismic and tectonic activities, including earthquakes, landslides, volcanic, tsunami, and anthropogenic effects, including land subsidence and mining. Deformation can be measured in terrestrial and non-terrestrial terms. Terrestrially, Global Navigation Satellite System (GNSS) and leveling surveys are considered the most reliable way to measure and detect deformation due to their high accuracy, but this method lacks precision data in a large area, much effort, and time data continuity. On the other hand, there are non-terrestrial methods with long data continuity, complete data coverage, and minimal operator interaction [8], [9]. The non-terrestrial method with remote sensing to detect deformations is generally known as Differential Interferometry Synthetic Aperture Radar (DInSAR) [10]. DInSAR is one of the

geodetic techniques using remote sensing satellites for providing high-resolution deformation measurements offering a high level of precision data over a large area but with less accuracy. This technique can be used to complement the lack of available field survey data which exists [8].

DInSAR is an active remote sensing technique based on the principle to analyze the paired SAR images that have been co-registered with different acquisition times to detect displacement of up to sub-centimeters along the sensor observation line to the target or Line of Sight (LOS) [11]. DInSAR provides high-resolution deformation measurements offering a high level of data precision over a large area but with less accuracy, so this technique can complement the lack of available field survey data [9]. By comparing 2 different SAR images, if there is a change on the earth's surface with the same location, the sensor will change the location of the point and consider the phase shift to generate an interferogram [12,13]. DInSAR can be used to monitor deformations related to various disaster phenomena such as earthquakes [14-16], volcanoes [17], land subsidence [18,19], and landslides [20]. Deformation monitoring is essential to support security aspects and regional planning, especially in areas with a high level of deformation, such as the Sunda Strait.

Sentinel-1 is a SAR satellite from the European Space Agency (ESA), an ongoing mission from the ESA project with ERS-1, ERS-2 ENVISAT, and Canada mission in RADARSAT-1 and RADARSAT-2 [21]. This satellite is a part of the Copernicus mission, which forms Sentinel-1, Sentinel-2, Sentinel-3, Sentinel-4, Sentinel-5 dan Sentinel-5p. The Sentinel-1 mission consists of a constellation of two satellites with polar orbits, operational during the day and night, and using C-band sensors [22]. C-band sensor in radar satellite has a wavelength (λ) of 5.66 cm, which allows the sensor to obtain backscattering from the surface of the subject and, at the same time, get additional backscattering from inside the object [22]. The acquisition of Sentinel-1 consists of several methods, including SM, IW, EW, and WV, each of which has its swath width and resolution (**Table 1**).

Table 1 Specification of Sentinel-1 acquisition modes.

Mode	Swat width	Resolution rg×az	Pixel spacing rg×az
Strip map (SM)	80 km	1.7×4.3 m to 3.6×4.9 m	1.5×3.6 m to 3.1×4.1 m
Interferometric Wide (IW)	250 km	2.7×22 m to 3.5×22 m	2.3×14.1 m
Extra-wide (EW)	400 km	7.9×43 to 1.5 to 43 m	5.9×19.9 m
Wave (WV)	20 km	2.0×4.8 m and 3.1×4.8 m	1.7×4.1 m and 2.7×4.1 m

Source: ESA (2020b).

Interferometric Wide (IW) is a Sentinel-1 data acquisition mode that is suitable to use in interferometry applications due to swath width and spatial resolution, specifically this mode for deformation monitoring. Besides, the availability of image data can be obtained for free [23]. The availability of Sentinel-1 data that is open public for a reasonably short period was chosen for use in this study. By applying the DInSAR method and Sentinel-1 imageries, this research is conducted to monitor dynamics deformation in the Sunda Strait region in 2019.

Materials and methods

Study area

Sunda Strait is a strait among Java Island, and Sumatra Island has had a complex tectonic structure and active seismic activity over the past 40 years (**Figure 1**). This area is changing the subduction system from the oblique subduction transitional zone between the Eurasian Plate and the Indo-Australian plate along the island of Sumatra to the frontal subduction of Java [1].

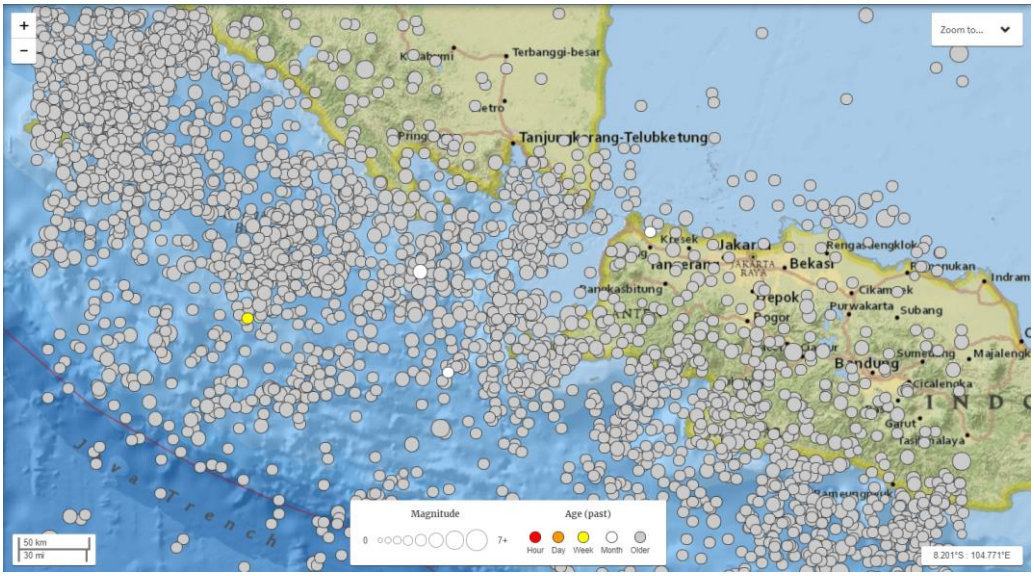

Figure 1 Seismic activity along the subduction zone in the Sunda strait is based on the USGS-NEIC catalog from 1980 to 2020 [24].

In this study, the west side of the Sunda Strait is chosen as the study area with its scope covering the Province of Lampung, especially around the Semangko Bay, Lampung Bay to Mount Anak Krakatau (**Figure 2**). A pair of Sentinel-1 descending images are used on a path row to extract deformation information in this region.

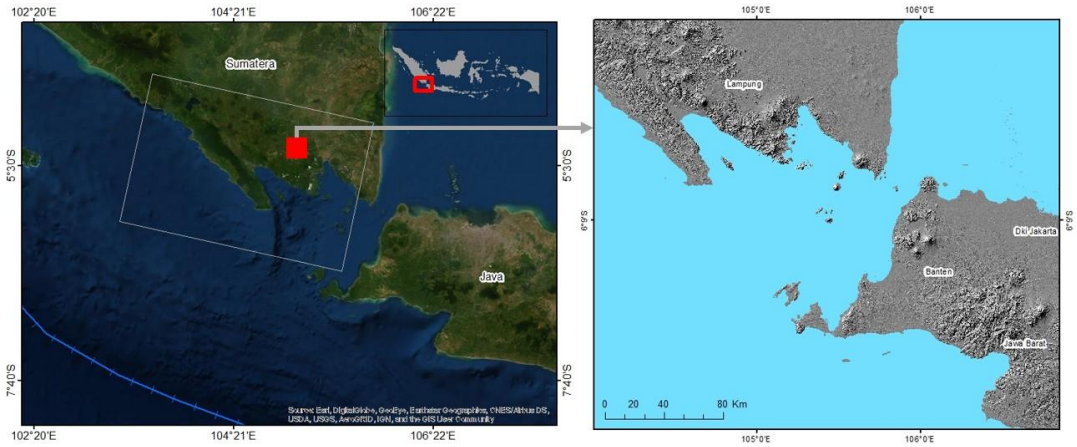

Figure 2 Study area and Sentinel-1 descending image coverage.

Research methodology

This section describes the method used to detect deformation in the area around the Sunda Strait. The flow chart is explained in **Figure 3**. This research uses the DInSAR approach based on the interferogram obtained from radar images in 2 acquisition times. The study area is around the Sunda Strait with a study focus on the western of the Sunda Strait covering the Province of Lampung, especially from the Semangko Bay, Lampung Bay to Mount Anak Krakatau. The SAR data used is a pair of Sentinel-1 descending imagery on June 1, 2019, and October 23, 2019.

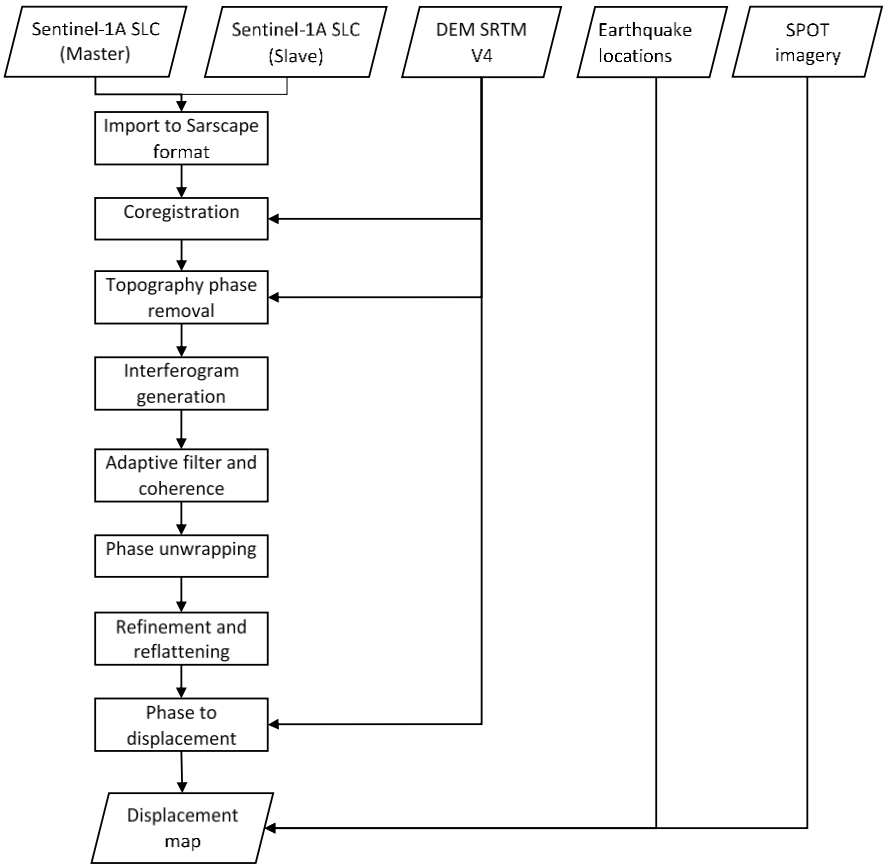

Figure 3 Dynamic displacement (deformation) processing using the DInSAR method.

Deformation processing is carried out with the initial stages of selecting a Sentinel-1 Single Look Complex (SLC) image pair with a small baseline to obtain high sensitivity to changes and limit the spatial decorrelation. Due to the distinctive acquisition time between master and slave images, the satellite's orbital is not precisely similar. The co-registration process is carried out from the image pair to get interferogram information to perform geometric co-registration of images using DEM data, orbit information, and correct residual shifts in the range and azimuth obtained from SAR data. The topographic effect was removed using topography phase removal by subtracting errors when the topography phase is removed from the local topography [25], this operation is done by the SRTM DEM data. After the topographic effect is removed and the orbital difference is fixed, the phase difference is generated from interferogram generation.

For removing noise and smoothing the interferogram, adaptive filter and coherence were applied to the Goldstein-Werner filtering. The phase unwrapping process in DInSAR performed is a step of recovering the actual value of phase difference by removing 2π discontinuities located on the interferogram, because of the distinction in the distances by the signals received by 2 SAR antennas, from the "wrapped" phase difference value [26].

Refinement and re-flattening step applied to correct change of the unwrapped phase information into displacement values. It permits both to refine the orbits and to figure the phase offset or eliminate phase ramps. Finally, the last value is converted to displacement and geocoded by the Range-Doppler approach into a map projection using the phase to displacement step. All processing and analyses were done by the SARscape® modules for ENVI 5.2.

Results and discussion

Perpendicular and temporal baseline

Image pair selection is an essential step in the measurement of ground surface deformations using the DInSAR method. The used selection criteria are the similarity of the orbit number, which indicates the same orbit location, the length of the perpendicular baseline, and the time interval between the 2 images. The higher the perpendicular baseline, the more accurate the topography dan displacement results [27].

Meanwhile, the longer time interval will reduce the coherence value [28]. In this study, the perpendicular baseline length was measured on 3 pairs of images in which 1 master image and 3 slave images. The results show that the highest perpendicular baselines in the image pair are the image pair with October 23, 2019. The shortest time interval is also on the image pair with October 23, 2019, slave image.

Table 2 Length of the perpendicular baseline and time interval of the images.

Master image ID scene	Slave image ID scene	Acquisition time	Baseline perpendicular (m)	Time interval (days)
Sentinel-1A June 1, 2019	Sentinel-1A October 23, 2019	October 23, 2019	−120.641	144
	Sentinel-1A November 16, 2019	November 16, 2019	43.8745	168
	Sentinel-1A December 10, 2019	December 12, 2019	−63.2307	192

Coherence

DInSAR principle is based on the Coherence change detection, which is based on radar intensity and phase differences between 2 temporally different SAR images. It is used in numerous applications, especially in ground surface deformation. The Coherence of 2 temporally different SAR images indicates the stability of the study area. The coherence value of the image pair has ranged from 0 to 1. Value 0 displays less similarity of both images, and value 1 shows identical of both images. The coherence histogram in **Figure 4** shows that the image pair used on June 1, 2019, and October 23, 2019, shows a difference in the coherence and less stable image pair, which meets the displacement analysis criteria.

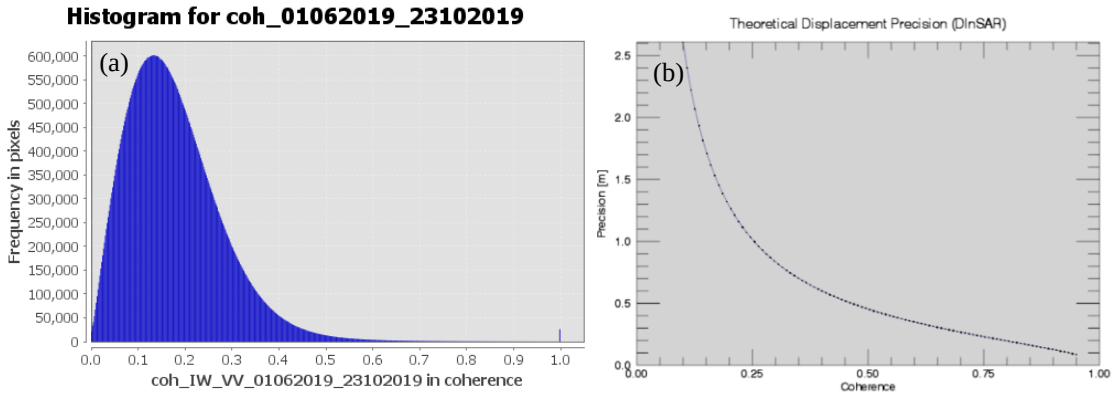

Figure 4 DInSAR coherence histograms of the study area (a) Coherence vs. frequency in pixels (b) Coherence vs. precision (m).

Interferogram

The results of the phase to the displacement of the DInSAR interferogram are in the form of LOS displacement, which is the surface change along the sensor observation line to the target [29]. From the June 1, 2019, and October 23, 2019 image pairs, a maximum uplift value of 0.54 m is obtained while the maximum subsidence value is −0.3 m. The location of the maximum uplift occurred in West Lampung Regency. Besides, uplift also occurred in Pesawaran and Lampung Timur Regency (**Figure 5**). The subsidence is located in the Pesisir Barat Regency and appears in several locations.

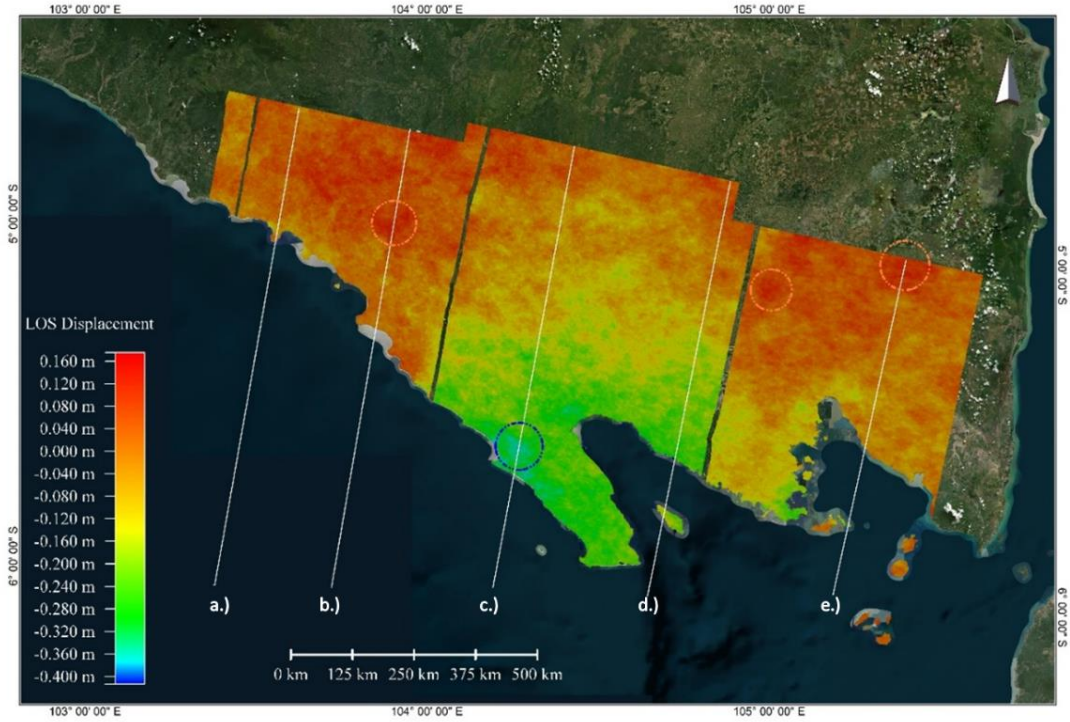

Figure 5 LOS displacement from June 2019 – to October 2019 (Orange circle: uplift, blue circle: subsidence).

1) Cross-section graph a
2)

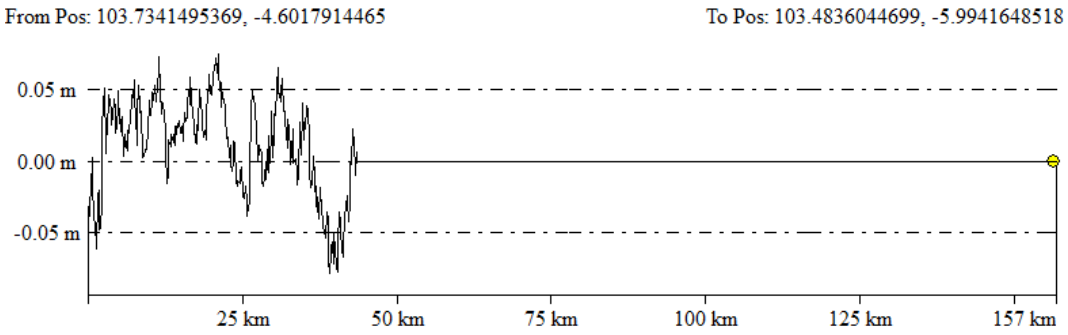

2) Cross-section graph b

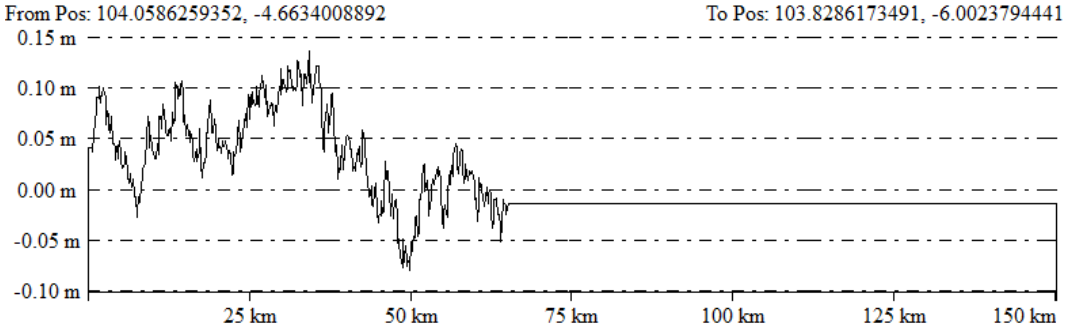

3) Cross-section c

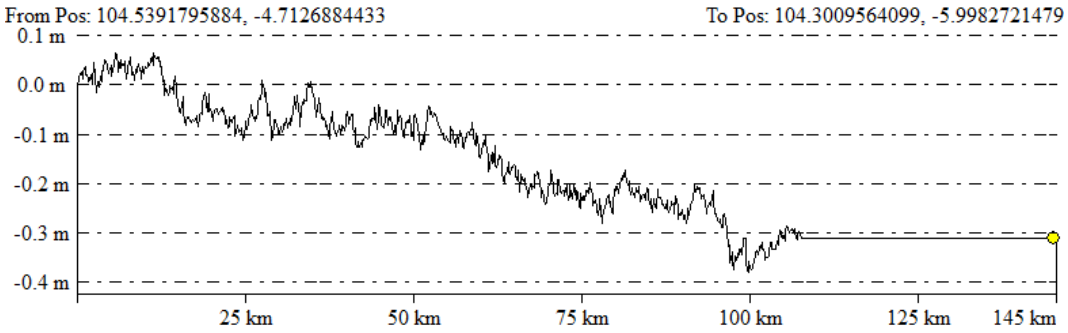

4) Cross-section graph d

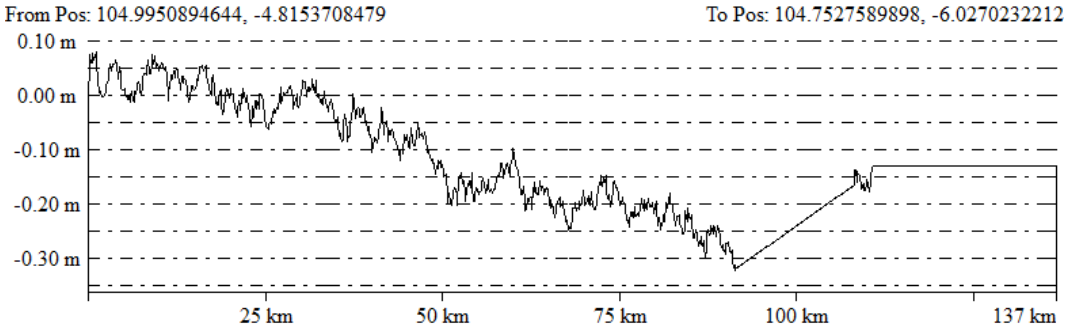

5) Cross-section graph e

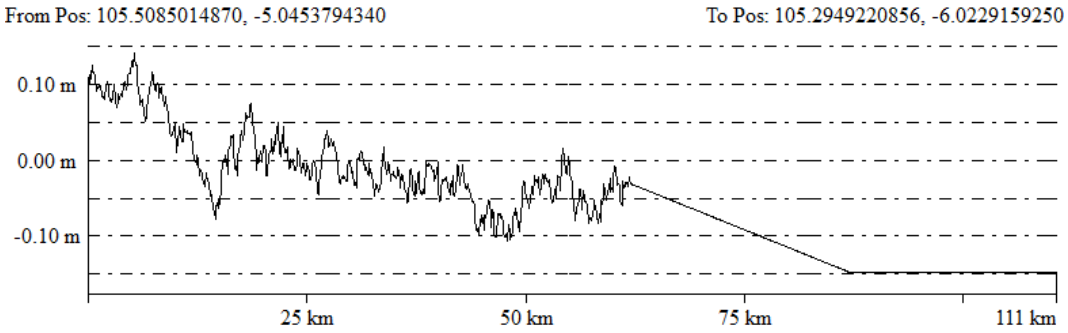

Figure 6 Cross-section graphic from phase to the displacement of June 2019 and October 2019 image pair.

The cross-section profile graph of the LOS displacement is presented in **Figure 6**. This cross-section graph emphasizes the uplift and land subsidence events shown in **Figure 6**. Cross-sections a and d are drawn at locations where there is no significant uplift or subsidence. Cross-sections b and e are found in locations where uplift occurs relatively high compared to the surrounding area. Furthermore, cross-section c passes through locations with subsidence events.

Geographic conditions

According to [30], in the Sunda Strait, there have been 15 earthquakes with a magnitude of more than five, in the period June 1, 2019, to October 23, 2019 (**Figure 7(a)**). However, most of the earthquake locations that occurred were not near the location of the displacement detected from the DInSAR analysis. At the land subsidence location, three earthquake events are located relatively close. From the land cover

conditions, the geographical condition of the displacement area can be seen in **Figures 7(b) - 7(d)**. In areas detected for uplift, the location is located in the mountains and plateaus with the general land cover in the form of dense vegetation and residential areas that are seen to be developing (**Figures 7(b) – 7(d)**). The location of land subsidence is located in the coastal areas where the conditions of settlements, agricultural land, and ponds have been seen are complete, although the vegetation is quite dense in the western area of the location.

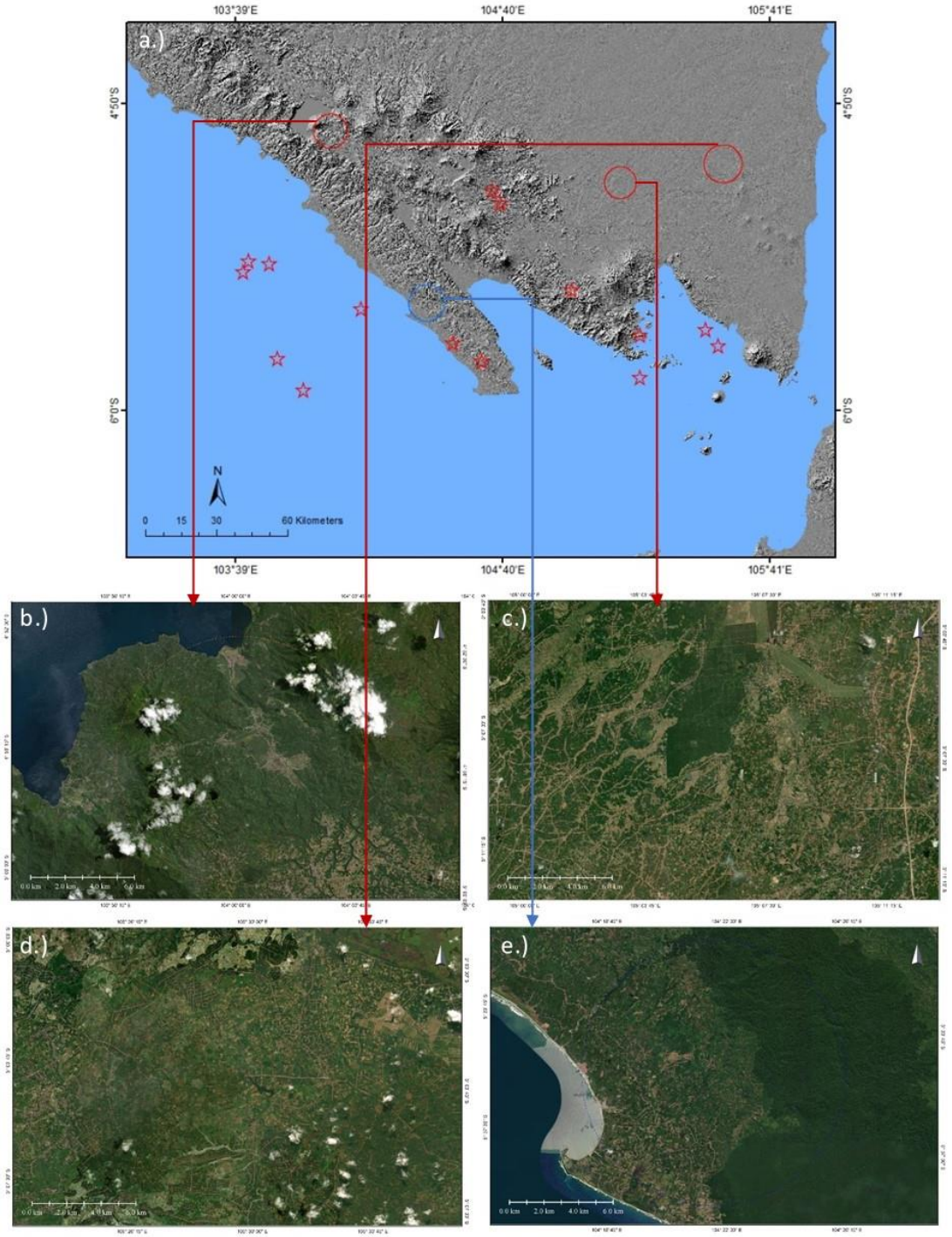

Figure 7 Geographic and seismic conditions from each displacement result. (a) Topographic and earthquake events from June - October 2019, (b) land use condition from uplift 1, (c) land use condition from uplift 2, (d) land use condition from uplift 3, e.) Land use condition from uplift 3, (e) Land use condition from land subsidence [30,31].

Discussion

The selection of image pairs is essential for analyzing ground deformation using DInSAR. The larger the perpendicular used, the more accurate the estimate of the topography, as clarified by the equation that relates the standard deviation of the phase measurement to the standard deviation of the DInSAR driven height measurements [27]. The standard deviation of the InSAR has driven height measurements, namely σ_z;

$$\sigma_z = -\frac{\lambda r}{4\pi}\frac{\sin\vartheta}{b_\perp}\sigma_\varphi \quad (1)$$

The histogram graphic of the coherence results shows that the highest coherence frequency in the used image pair is at Coherence from 0.1 to 0.2, which indicates the minimum similarity conditions of the 2 images. The low value of coherence is due to differences in the phase and intensity values of the SAR image pair used. Phase and image intensity differences between two image pairs can be caused by changes in conditions by deformation and change in a regional scale area. The regional change can be caused by land-use change.

Based on the seismic events recorded at the scene during the image pair acquisition period, there were no close and significant seismic events. Although there were three earthquake events with a magnitude above 5 near the location where land subsidence was detected, a considerable distance from the location makes displacement less influenced by seismic activity.

Based on the geological map of Tanjung Karang, geological conditions from uplift areas are dominated with rick by type Tuff sandstone (Qtl), Hollow Basalt (Qbs), sandstone with claystone (Qpt), and natural stone. Cross-sections of the uplift areas are shown in **Figures 6(b)** and **6(e)** where these figures indicated that the uplift location is relatively higher than the surrounding areas. Furthermore, from the geographical conditions, the uplift area is mostly in the form of vegetation with a high-density level so that the detected uplift may be due to changes in the vegetation conditions in the area of uplift occurrence. It is consistent with the results obtained by [34] that the vegetation affects displacement analysis from DInSAR.

On the other hand, based on the geological map of Kota Agung, the geological condition of the land subsidence detected areas are dominated by Tufan sandstone (Tmps), alluvium (Qa), and a little volcanic breccias. Geographical conditions of this area located in the coastal area and settlements, agriculture, and ponds are dominated the land used. This condition is supported by **Figure 7(c)** where the land subsidence location is relatively lower altitude than the surrounding area. The geographical and geological conditions of the area mentioned above are very closely related if land subsidence occurs. This result is supported by research by [32], [33], where land subsidence is located in the alluvial plain and affected by alluvial consolidation and groundwater extraction.

Deformation detection results by DInSAR are in the form of LOS displacement so that the actual conditions in the field are not necessarily by the results obtained. So, it is necessary to verify the conditions in the field to ensure the uplift and land subsidence events that have been obtained from the DInSAR analysis.

Conclusions

Based on the processing and analysis of the results that have been carried out, it can be concluded that Lampung Province in Sunda Strait has experienced uplift and land subsidence in several locations. These phenomena are affected by the conditions of the location, which have active seismic activity and an active fault called the Semangko fault. DInSAR method can detect displacement using the principle of coherence change detection based on radar intensity and phase differences between two temporally different SAR images.

The dynamic of uplift and subsidence in the Lampung Province is mainly affected by the locations' geological and land cover conditions. The displacement by DInSAR has resulted in the LOS displacement, so that in the present necessary to monitor the displacement continuously and verify the conditions in the field to ensure the uplift and land subsidence events.

Acknowledgments

The author would like to thank *European Space Agency* (ESA) for providing Sentinel-1 data and the Indonesian Institute of Aeronautics and Space (LAPAN - currently BRIN) for supporting this research on the implementation of this research. We thank anonymous reviewers. Argo Galih Suhadha contributed to conceptualizing, methodology, data processing, analyzing, and writing. Atriyon Julzarika contributed to analyzing, method, data validating, and writing.

References

[1] M Abdurrachman, S Widiyantoro, B Priadi and T Ismail. Geochemistry and structure of krakatoa volcano in the Sunda Strait, Indonesia. *Geosciences* 2018; **8**, 111.

[2] A Julzarika, DP Laksono, L Subehi, EK Dewi, K Kayat, HA Sofiyuddin and MFI Nugraha. Comprehensive integration system of saltwater environment on Rote Island using a multidisciplinary approach. *J. Degraded Min. Lands Manag.* 2018; **6**, 1553-67.

[3] KR Newcomb and WR Mccann. Seismic history and seismotectonics of the Sunda Arc. *J. Geophys. Res.* 1987; **92**, 421-39.

[4] AG Suhadha and A Julzarika. Integration of remote sensing and geographic information system for mapping potential tsunami inundation. *In*: Proceedings of the 2020 IEEE Asia-Pacific Conference on Geoscience, Electronics and Remote Sensing Technology, Jakarta, Indonesia. 2020, p. 163-7.

[5] LD Setijadji. Segmented volcanic arc and its association with geothermal fields in Java Island, Indonesia. *In*: Proceedings of the proceedings world geothermal congress 2010, Bali, Indonesia. 2010.

[6] KE Bradley, L Feng, EM Hill, DH Natawidjaja and K Sieh. Implications of the diffuse deformation of the indian ocean lithosphere for slip partitioning of oblique plate convergence in Sumatra. *J. Geophys. Res.* 2017; **122**, 579-91.

[7] R Williams, P Rowley and MC Garthwaite. Reconstructing the anak krakatau flank collapse that caused the december 2018 indonesian tsunami. *Geology* 2019; **47**, 973-6.

[8] HZ Abidin, H Andreas, I Gumilar, TP Sidiq and Y Fukuda. *On the roles of geospatial information for risk assessment of land subsidence in urban areas of Indonesia*. *In*: S Zlatanova, R Peters, A Dilo and H Scholten (Eds.). Intelligent systems for crisis management. Springer Science & Business Media, Berlin, Germany, 2013, p. 277-88.

[9] I Gumilar, HZ Abidin, TP Sidiq, H Andreas, R Maiyudi and M Gamal. Mapping and evaluating the impact of land subsidence in semarang (indonesia). *Indonesian J. Geospatial* 2013; **2**, 26-41.

[10] A Ferretti. *Satellite InSAR data: Reservoir monitoring from space*. European Association of Geoscientists and Engineers, Kuala Lumpur, Malaysia, 2014, p. 1-160.

[11] Q Huang, M Crosetto, O Monserrat and B Crippa. Displacement monitoring and modelling of a high-speed railway bridge using C-band Sentinel-1 data. *ISPRS J. Photogram Rem. Sens.* 2017; **128**, 204-11.

[12] P Jeanne, M Crosetto, O Monserrat and B Crippa. Role of agricultural activity on land subsidence in the san joaquin valley, california. *J. Hydrol.* 2018; **569**, 462-9.

[13] S Schindler, F Hegemann, C Koch, M König and P Mark. Radar interferometry based settlement monitoring in tunnelling: Visualisation and accuracy analyses. *Visual. Eng.* 2016; **4**, 7.

[14] A Aditiya, Y Aoki and RD Anugrah. Surface deformation monitoring of Sinabung volcano using multi temporal InSAR method and GIS analysis for affected area assessment. *IOP Conf. Ser. Earth Environ. Sci.* 2018; **344**, 012003.

[15] A Agustan, RN Hanifa, Y Anantasena, M Sadly and T Ito. Ground deformation identification related to 2018 lombok earthquake series based on Sentinel-1 data. *IOP Conf. Ser. Earth Environ. Sci.* 2019; **280**, 012004.

[16] AG Suhadha, A Julzarika, M Ardha and F Chusnayah. Monitoring vertical deformations of the coastal city of palu after earthquake 2018 using Parallel-SBAS. *In*: Proceedings of the 2021 7th Asia-Pacific Conference on Synthetic Aperture Radar, Bali, Indonesia. 2021.

[17] AM Lubis. Uplift of kelud volcano prior to the november 2007 eruption as observed by L-band insar. *J. Eng. Technol. Sci.* 2014; **46**, 245-57.

[18] J Widodo, A Herlambang, A Sulaiman and P Razi. Land subsidence rate analysis of jakarta metropolitan region based on D-InSAR processing of sentinel data C-Band frequency land subsidence rate analysis of jakarta metropolitan region based on D-InSAR processing of sentinel data C-Band frequency. *J. Phys. Conf. Ser.* 2019; **1185**, 012004.

[19] M Ardha, AG Suhadha, A Julzarika, F Yulianto, D Yudhatama and RZ Darwista. Utilization of sentinel-1 satellite imagery data to support land subsidence analysis in DKI Jakarta. *J. Degraded Min. Lands Manag.* 2021; **8**, 2587-93.
[20] M Tzouvaras, C Danezis and DG Hadjimitsis. Differential SAR interferometry using sentinel-1 imagery-limitations in monitoring fast moving landslides: The case study of cyprus. *Geosciences* 2020; **10**, 1-25.
[21] European Space Agency. Sentinel-1 heritage 2020, Available at: https://sentinel.esa.int/web/sentinel/missions/sentinel-1/heritage, accessed May 2020.
[22] European Space Agency. Sentinel-1 mission 2020, Available at: https://sentinel.esa.int/web/sentinel/missions/sentinel-1, accessed May 2020.
[23] A Sowter, MBC Amat, F Cigna, S Marsh, A Athab and L Alshammari. Mexico city land subsidence in 2014-2015 with Sentinel-1 IW TOPS: Results using the intermittent SBAS (ISBAS) technique. *Int. J. Appl. Earth Observation Geoinformation* 2016; **52**, 230-42.
[24] U.S. Geological Survey. EXPO-CAT earthquake catalog, earthquake catalog epicenters, Available at: http://earthquake.usgs.gov/research/pager/data/expocat.php, accessed May 2020.
[25] N Liosis, PR Marpu, K Pavlopoulos and TBMJ Ouarda. Ground subsidence monitoring with SAR interferometry techniques in the rural area of Al Wagan, UAE. *Rem. Sens. Environ.* 2018; **216**, 276-88.
[26] SN Madsen and HA Zebker. Automated absolute phase retrieval in. *In*: Proceedings of the IGARSS' 92 International Geoscience and Remote Sensing Symposium, Texas, United States. 1992, p. 1582-4.
[27] A Pepe and F Calò. A review of interferometric synthetic aperture RADAR (InSAR) multi-track approaches for the retrieval of Earth's surface displacements. *Appl. Sci.* 2017; **7**, 1264.
[28] IM Anjasmara and NU Muthmainnah. Analisis deformasi pulau madura dari pengolahan data SAR menggunakan metode DInSAR. *Geoid J. Geodes. Geomatics* 2018; **14**, 103.
[29] D Massonnet and KL Feigl. Radar interferometry and its application to changes in the earth's surface. *Rev. Geophys.* 1998; **36**, 441-500.
[30] Badan Meteorologi, Klimatologi, dan Geofisika. Repository gempabumi, Available at: http://repogempa.bmkg.go.id/repo_new/repository.php, accessed June 2020.
[31] ESRI database 2020, Available at: http://goto.arcgisonline.com/maps/World_Imagery, accessed June 2020.
[32] S Widada, M Zainuri, G Yulianto, S Saputra and B Rochaddi. Distributian of depth and clay-silt to sand ratio of land subsidence in coastal semarang city by resistivity methods. *J. Kelautan Tropis* 2019; **22**, 63-8.
[33] HZ Abidin, H Andreas, I Gumilar, TP Sidiq and Y Fukuda. Land subsidence in coastal city of Semarang (Indonesia): Characteristics, impacts and causes. *Geomatics Nat. Hazards Risk* 2013; **4**, 226-40.